Correlational and thermodynamic properties of finite-temperature electron liquids in the hypernetted-chain approximation

Tanaka, Shigenori

(Citation)
Journal of Chemical Physics,145(21):214104-214104

(Issue Date)
2016-12-07

(Resource Type)
journal article

(Version)
Version of Record

Correlational and thermodynamic properties of finite-temperature electron liquids in the hypernetted-chain approximation

Shigenori Tanaka

Citation: J. Chem. Phys. **145**, 214104 (2016); doi: 10.1063/1.4969071
View online: http://dx.doi.org/10.1063/1.4969071
View Table of Contents: http://aip.scitation.org/toc/jcp/145/21
Published by the American Institute of Physics

Correlational and thermodynamic properties of finite-temperature electron liquids in the hypernetted-chain approximation

Shigenori Tanaka[a)]
Graduate School of System Informatics, Kobe University, 1-1 Rokkodai, Nada, Kobe 657-8501, Japan

(Received 28 September 2016; accepted 15 November 2016; published online 6 December 2016)

Correlational and thermodynamic properties of homogeneous electron liquids at finite temperatures are theoretically analyzed in terms of dielectric response formalism with the hypernetted-chain (HNC) approximation and its modified version. The static structure factor and the local-field correction to describe the strong Coulomb-coupling effects beyond the random-phase approximation are self-consistently calculated through solution to integral equations in the paramagnetic (spin unpolarized) and ferromagnetic (spin polarized) states. In the ground state with the normalized temperature $\theta = 0$, the present HNC scheme well reproduces the exchange-correlation energies obtained by quantum Monte Carlo (QMC) simulations over the whole fluid phase (the coupling constant $r_s \leq 100$), i.e., within 1% and 2% deviations from putative best QMC values in the paramagnetic and ferromagnetic states, respectively. As compared with earlier studies based on the Singwi-Tosi-Land-Sjölander and modified convolution approximations, some improvements on the correlation energies and the correlation functions including the compressibility sum rule are found in the intermediate to strong coupling regimes. When applied to the electron fluids at intermediate Fermi degeneracies ($\theta \approx 1$), the static structure factors calculated in the HNC scheme show good agreements with the results obtained by the path integral Monte Carlo (PIMC) simulation, while a small negative region in the radial distribution function is observed near the origin, which may be associated with a slight overestimation for the exchange-correlation hole in the HNC approximation. The interaction energies are calculated for various combinations of density and temperature parameters ranging from strong to weak degeneracy and from weak to strong coupling, and the HNC values are then parametrized as functions of r_s and θ. The HNC exchange-correlation free energies obtained through the coupling-constant integration show reasonable agreements with earlier results including the PIMC-based fitting over the whole fluid region at finite degeneracies in the paramagnetic state. In contrast, a systematic difference between the HNC and PIMC results is observed in the ferromagnetic state, which suggests a necessity of further studies on the exchange-correlation free energies from both aspects of analytical theory and simulation. *Published by AIP Publishing.* [http://dx.doi.org/10.1063/1.4969071]

I. INTRODUCTION

Recently, there has been an increasing interest in the thermodynamic properties of uniform electron gas or liquid systems at finite Fermi degeneracies, which play a pivotal role in warm dense matter (WDM)[1–4] characterized by elevated temperatures and wide compression ranges. A lot of astrophysical objects and materials under extreme experimental or environmental conditions are associated with the WDM, such as those highly compressed states observed in compact stars, planet cores, inertial confinement fusion, and laser ablation.[5] Theoretical descriptions by *ab initio* computer simulations for these materials are important both for interpreting experimental results and for obtaining insights into those parameter regions difficult to access experimentally, which could be performed in the framework of finite-temperature density functional theory (DFT).[3,4] In this formulation of finite-temperature DFT calculations, the accurate information on thermodynamics of electron fluid over a wide range of density and temperature is essential for constructing the input exchange-correlation potentials.

Substantial progress has been achieved since the 1980's in the theoretical study of the correlational and thermodynamic properties of uniform electron gas or liquid at finite temperatures.[5] The dielectric and thermodynamic functions have been calculated first in the random-phase approximation (RPA)[6–9] and next in the approaches involving the local-field correction (LFC)[5,10] which describes the strong-coupling effects beyond the RPA. The latter includes those self-consistent integral equation approaches based on the parametrized LFC,[11] the Singwi-Tosi-Land-Sjölander (STLS) approximation,[12–14] the dynamical STLS approximation,[15] the Vashishta-Singwi (VS) approximation,[16,17] and the modified convolution approximation (MCA).[10,18–20] Through comparison with the existing Monte Carlo simulation data in the classical and ground-state limits, these analytic approaches have been expected to provide fairly accurate predictions for the thermodynamic functions at any Fermi degeneracy of electrons, e.g., within several % deviations in the exchange-correlation free energies from the "true" values in the cases of STLS and MCA approximations.[13,14,20]

a)Electronic address: tanaka2@kobe-u.ac.jp

On the other hand, quantum Monte Carlo (QMC) simulations are in principle expected to provide the exact solution to the correlational and thermodynamic quantities of electron gas.[21] As for the finite-temperature uniform electron gas, Brown *et al.*[22] first applied the restricted path integral Monte Carlo (RPIMC) method in coordinate space to the evaluation of correlational and thermodynamic functions, in which the fermion nodes of density matrix were fixed at those of ideal Fermi gas to avoid the sign problem.[23] Brown *et al.*[24] also derived an analytic parametrization for the exchange-correlation free energy as a function of density and temperature of electron gas on the basis of their RPIMC data. Unfortunately, their simulation results have been found to contain some systematic errors especially in the low-temperature and high-density regimes, and the parametrized expression for thermodynamic functions shows unphysical behaviors due to its irrelevant functional form. Karasiev *et al.* (KSDT)[25] then proposed an improved fitting formula for the exchange-correlation free energy by performing appropriate interpolation with correct asymptotic limits. In addition, other path integral Monte Carlo (PIMC) calculations, the permutation blocking path integral Monte Carlo (PB-PIMC) approach with a higher-order factorization of density matrix,[26,27] and the configuration path integral Monte Carlo (CPIMC) approach formulated in the Fock space of Slater determinants[27,28] were also carried out to extend the validity of QMC calculations to wider parameter regions. However, the difficulties associated with the finite system size (typically 33 particles for spin-polarized case), the fermion sign problem, and the finite time slice still remain in spite of continuing efforts to overcome or correct them. (As for the latest advance in the finite-size correction, see a recent work by Dornheim *et al.*[29])

Considering the current situation that a completely dependable formula for the exchange-correlation free energy of an electron fluid over any combination of number density n, temperature T, and spin polarization ζ has not been obtained, the present study performs novel integral-equation-based calculations for the correlational and thermodynamic properties of finite-temperature electron liquids on the basis of the hypernetted-chain (HNC) approximation, which is expected to give better correlation and thermodynamic functions than the earlier approaches[13,14,20] with comparable accuracy to the simulation results. The HNC approximation is known to provide very accurate descriptions for the correlational and thermodynamic properties of classical one-component plasma (OCP) over the whole fluid region.[5,10,30–32] We here take into account the HNC approximation in the framework of the dielectric, density-response formalism at finite temperatures[5] which would allow for accurate descriptions both in the weak-coupling (Hartree-Fock and RPA) and strong-coupling (nearly crystalline) regimes. We thus calculate the normalized interaction energies per electron in units of the Coulomb energy (e^2/a; see below) over the wide range of density and temperature in the fluid-phase, spin unpolarized (paramagnetic) and polarized (ferromagnetic) states. In addition, parametrized expressions for the normalized interaction energies and the exchange-correlation free energies are derived, which would be accurate over the whole fluid region of finite-temperature (including the ground-state and classical limits) electron gas or liquid, supposing the smooth interpolation for the normalized interaction energies. Besides, it is noted that the present HNC scheme on the basis of the dielectric formulation with the LFC[5,10,33] is different from the classical-map HNC (CHNC) approach[34–37] in which the correspondence to the classical system is utilized and also different from the Fermi-HNC approach[38,39] in which the variational principle with respect to the ground-state energy is employed.

In the following, the theoretical framework of this work is first illustrated in Sec. II. Calculational results are then shown in Sec. III with associated discussions. Conclusions and some additional remarks are given in Sec. IV.

II. THEORY

A. Physical parameters

Let us consider a homogeneous electron fluid with the average number density $n = N/V$ and the absolute temperature T with N and V being the particle number and the volume. The Coulomb coupling constant for the degenerate electron gas or liquid is given by[5,10]

$$r_s = a/a_B, \tag{1}$$

where $a = (3/4\pi n)^{1/3}$ is the Wigner-Seitz radius and $a_B = \hbar^2/me^2$ is the Bohr radius with $\hbar$, m, and $-e$ being the Planck constant, the mass, and electric charge of an electron, respectively. In the high-temperature, classical limit, the strength of Coulomb coupling can instead be measured by[5,10]

$$\Gamma = \frac{e^2}{ak_BT}, \tag{2}$$

where k_B refers to the Boltzmann constant. The degree of Fermi degeneracy is then measured by[5,10]

$$\theta = k_BT/E_F, \tag{3}$$

where $E_F = \hbar^2k_F^2/2m$ is the Fermi energy with $k_F = (3\pi^2n)^{1/3}$ being the Fermi wavenumber. It is noted that the common E_F with k_F (not with $k_F' = (6\pi^2n)^{1/3}$) is employed both for the paramagnetic and ferromagnetic states in the present study, thus θ is determined only in terms of T and n. There is a useful relation among the three parameters, r_s, Γ, and θ as

$$\Gamma\theta = 2\lambda^2 r_s \tag{4}$$

with $\lambda = (4/9\pi)^{1/3}$. Moreover, the degree of spin polarization in the electron fluid is measured by[20]

$$\zeta = (n_1 - n_2)/n, \tag{5}$$

where n_1 and n_2 represent the number densities of spin-up and spin-down electrons, respectively, hence $\zeta = 0$ for the paramagnetic (spin unpolarized) state and $\zeta = 1$ for the ferromagnetic (spin polarized) state.

B. Density response formalism

We start with the fluctuation-dissipation relation between the wavenumber (k)- and frequency (ω)-dependent, retarded density response function $\chi_+(k,\omega)$ and the dynamic structure factor $S(k,\omega)$ as[5,13]

$$S(k,\omega) = -\frac{\hbar}{2\pi}\coth\left(\frac{\hbar\omega}{2k_BT}\right)\mathrm{Im}\,\chi_+(k,\omega). \tag{6}$$

The static structure factor is then obtained through the principal value ($\wp$) integral over the frequency of $S(k,\omega)$ as

$$S(k) = -\frac{\hbar}{2\pi n}\,\wp\int_{-\infty}^{\infty} d\omega\,\coth\left(\frac{\hbar\omega}{2k_BT}\right)\mathrm{Im}\,\chi_+(k,\omega)$$
$$= -\frac{k_BT}{n}\sum_{l=-\infty}^{\infty}\chi(k,z_l), \tag{7}$$

where the contributions from the discrete frequencies $z_l = 2\pi i l k_BT/\hbar\,(l = 0, \pm1, \pm2, \ldots)$ on the imaginary axis have been summed after the deformation of the integral contour.[13] The complex-frequency-dependent, causal density response function is expressed in the density response formalism as[5]

$$\chi(k,z) = \frac{\chi_0(k,z)}{1 - v(k)\,[1 - G(k,z)]\,\chi_0(k,z)}, \tag{8}$$

where $v(k) = 4\pi e^2/k^2$ and the free-particle polarizability of electrons,

$$\chi_0(k,\omega) = \sum_{\sigma}\sum_{\boldsymbol{q}}\frac{f_\sigma(\boldsymbol{q}) - f_\sigma(\boldsymbol{q}+\boldsymbol{k})}{\hbar\omega + \epsilon(\boldsymbol{q}) - \epsilon(\boldsymbol{q}+\boldsymbol{k}) + i\delta}, \tag{9}$$

have been introduced with $\epsilon(q) = \hbar^2q^2/2m$ and $\delta \to +0$; the Fermi distribution function for each spin species σ (up and down)

$$f_\sigma(q) = \left\{\exp\left[\frac{\epsilon(q)}{k_BT} - \alpha_\sigma\right] + 1\right\}^{-1} \tag{10}$$

with the dimensionless chemical potential α_σ satisfies the normalization condition

$$n_\sigma = \sum_{\boldsymbol{k}} f_\sigma(\boldsymbol{k}) \tag{11}$$

with $n = \sum_\sigma n_\sigma$, where we use a conventional notation,

$$\sum_{\boldsymbol{k}} = \int\frac{d\boldsymbol{k}}{(2\pi)^3}. \tag{12}$$

If we set $G(k,z) = 0$ in Eq. (8), we recover the random-phase approximation (RPA) expression for the density response function. The local-field correction (LFC) $G(k,z)$ thus accounts for the strong-coupling effects beyond the RPA[5,10] and plays an essential role to accurately describe the correlational and thermodynamic properties of electron liquids.

C. Hypernetted-chain (HNC) approximation

In this subsection we derive a relation between the LFC and the static structure factor in the HNC approximation, thus providing a closure equation to determine them self-consistently in the wavenumber (k) space. Hereafter, we rely on the static approximation to the LFC, i.e., $G(k,z) \simeq G(k)$, and the static $G(k)$ is related to $S(k)$ on the basis of classical liquid theory.

Let us note a relation between the static structure factor and the static density response function as[10,30]

$$S(k) = -\frac{k_BT}{n}\chi(k,0) \tag{13}$$

in the classical limit ($\theta \to \infty$). The static density response function is then written as

$$\chi(k,0) = \frac{\chi_0(k,0)}{1 - v(k)\,[1 - G(k)]\,\chi_0(k,0)} \tag{14}$$

with

$$\chi_0(k,0) = -\frac{n}{k_BT}. \tag{15}$$

The Ornstein-Zernike relation between the pair correlation function $h(r)$ and the direct correlation function $c(r)$ in classical simple liquids,[30]

$$h(r) = c(r) + n\int d\boldsymbol{r}'c(\boldsymbol{r}-\boldsymbol{r}')h(\boldsymbol{r}'), \tag{16}$$

is expressed as

$$\hat{h}(k) = \hat{c}(k) + n\hat{c}(k)\hat{h}(k) \tag{17}$$

in the k-space, where we employ the Fourier transformation as

$$\hat{h}(k) = \int d\boldsymbol{r}e^{i\boldsymbol{k}\cdot\boldsymbol{r}}h(r) \tag{18}$$

for the pair correlation function and the analogous expression for the direct correlation function. Since the pair correlation function is related to the static structure factor as

$$S(k) = 1 + n\hat{h}(k), \tag{19}$$

we find a relation,

$$v(k)\,[1 - G(k)] = -k_BT\hat{c}(k), \tag{20}$$

through comparison between Eqs. (13) and (17).

The HNC equation for classical simple liquids reads[30]

$$h(r) + 1 = \exp\left[-\frac{V(r)}{k_BT} + h(r) - c(r)\right] \tag{21}$$

with $V(r) = e^2/r$ in the case of electron liquid. This equation is rewritten as

$$c(r) = \exp\left[-\frac{V(r)}{k_BT} + n\int d\boldsymbol{r}'c(\boldsymbol{r}-\boldsymbol{r}')h(\boldsymbol{r}')\right]$$
$$- n\int d\boldsymbol{r}'c(\boldsymbol{r}-\boldsymbol{r}')h(\boldsymbol{r}') - 1 \tag{22}$$

with the use of the Ornstein-Zernike relation, Eq. (16). We here take the gradient of $\boldsymbol{r}$ over both the sides of this equation, thus finding

$$\nabla c(r) = -\frac{\nabla V(r)}{k_BT}\,[h(r) + 1] + nh(r)\int d\boldsymbol{r}'\nabla c(\boldsymbol{r}-\boldsymbol{r}')h(\boldsymbol{r}'). \tag{23}$$

Fourier transformation of this equation and the operation of $i\boldsymbol{k}$ then lead to[33]

$$k^2\left[\hat{c}(k) + \frac{v(k)}{k_BT}\right] = -\frac{1}{k_BT}\sum_{\boldsymbol{q}}\boldsymbol{k}\cdot\boldsymbol{q}\hat{h}(\boldsymbol{k}-\boldsymbol{q})v(\boldsymbol{q})$$
$$+ n\sum_{\boldsymbol{q}}\boldsymbol{k}\cdot\boldsymbol{q}\hat{h}(\boldsymbol{k}-\boldsymbol{q})\hat{h}(\boldsymbol{q})\hat{c}(\boldsymbol{q}). \tag{24}$$

With the aid of Eqs. (19) and (20), we thus obtain

$$G(k) = -\frac{1}{n}\sum_{\boldsymbol{q}}\frac{\boldsymbol{k}\cdot\boldsymbol{q}}{\boldsymbol{q}^2}\,[S(\boldsymbol{k}-\boldsymbol{q}) - 1]$$
$$\times\,\{1 - [G(\boldsymbol{q}) - 1]\,[S(\boldsymbol{q}) - 1]\}. \tag{25}$$

This LFC form in the HNC approximation is reduced to two well-known expressions, the STLS and convolution approximation (CA) types,[10] as limiting cases. If we set $G(q) = 1$ on the right-hand side of Eq. (25), we recover the STLS expression of LFC. On the other hand, if we set $G(q) = 0$, we

recover the CA expression. Considering this property, we here divide the LFC into two parts as

$$G(k) = G_1(k) + G_2(k) \tag{26}$$

with

$$G_1(k) = -\frac{1}{n}\sum_{\boldsymbol{q}} \frac{\boldsymbol{k}\cdot\boldsymbol{q}}{\boldsymbol{q}^2}\left[S(\boldsymbol{k}-\boldsymbol{q}) - 1\right] \tag{27}$$

and

$$G_2(k) = \frac{1}{n}\sum_{\boldsymbol{q}} \frac{\boldsymbol{k}\cdot\boldsymbol{q}}{\boldsymbol{q}^2}\left[S(\boldsymbol{k}-\boldsymbol{q}) - 1\right]\left[G(\boldsymbol{q}) - 1\right]\left[S(\boldsymbol{q}) - 1\right]. \tag{28}$$

$G_1(k)$ represents the STLS part of LFC, and as seen in Sec. III, $G_2(k)$ refers to a small correction to $G_1(k)$ in the long-wavelength region.

In addition to the HNC approximation above, another approximation called the modified hypernetted-chain (MHNC) approximation is examined in the present study. On the basis of an analogous idea to the MCA[18–20] in which some improvements on the correlational and thermodynamic properties over the CA have been observed, $S(\boldsymbol{k}-\boldsymbol{q})$ in Eq. (28) is replaced with a screening function defined by

$$\overline{S}(k) = \frac{k^2}{k^2 + k_s^2}, \tag{29}$$

so that the second term of LFC in the MHNC approximation is given by

$$\overline{G}_2(k) = \frac{1}{n}\sum_{\boldsymbol{q}} \frac{\boldsymbol{k}\cdot\boldsymbol{q}}{\boldsymbol{q}^2}\left[\overline{S}(\boldsymbol{k}-\boldsymbol{q}) - 1\right]\left[G(\boldsymbol{q}) - 1\right]\left[S(\boldsymbol{q}) - 1\right]. \tag{30}$$

Performing the angular integration in Eq. (30), we obtain the expression for $\overline{G}_2(k)$ over a one-dimensional integral as

$$\overline{G}_2(k) = \frac{k_s^2}{(2\pi)^2 n}\int_0^\infty dq\left[1 + \frac{q^2 + k^2 + k_s^2}{4kq}\ln\left|\frac{(q-k)^2 + k_s^2}{(q+k)^2 + k_s^2}\right|\right] \times \left[G(q) - 1\right]\left[S(q) - 1\right]. \tag{31}$$

The screening wavenumber k_s is then determined self-consistently via a constraint as

$$\frac{1}{2}\sum_{\boldsymbol{k}} v(k)\left[\overline{S}(k) - 1\right] = \frac{1}{2}\sum_{\boldsymbol{k}} v(k)\left[S(k) - 1\right], \tag{32}$$

which implies that the interaction energy calculated from $\overline{S}(k)$ is identical to that from $S(k)$. Since $G_1(k)$ can also be calculated in terms of a one-dimensional integral, the total LFC in the MHNC approximation is expressed over the one-dimensional integration in the wavenumber space, which markedly reduces the computational cost and well retains the numerical stability concerning the convergence of solution to integral equations for $G(k)$ and $S(k)$. The MHNC solution to $G(k)$ can also be used as the initial input for solving the HNC integral equations.

III. RESULTS AND DISCUSSION

On the theoretical basis explained in Sec. II, we can obtain $G(k)$ and $S(k)$ through a self-consistent solution to the integral equations, Eqs. (7), (8), and (25), in the HNC approximation. In the case of MHNC approximation, Eq. (30) is employed for the $G_2(k)$ part instead of Eq. (28). The present approach is fully quantum-mechanical up to the approximation level of RPA. As for the description of the strong-coupling effect beyond the RPA, we rely on the classical HNC approximation for the static LFC $G(k)$.

A. Classical limit

First, we consider the classical limit, in which Eqs. (13)–(15) are used for the calculation of $S(k)$. It is known that the HNC approximation accurately describes the correlational and thermodynamic properties of the classical electron gas or the one-component plasma (OCP) in the whole fluid regime ($\Gamma \lesssim 200$).[5,10] Figure 1 illustrates the radial distribution function (RDF) at $\Gamma = 10$ calculated by

$$g(r) = 1 + h(r) = 1 + \frac{1}{n}\sum_{\boldsymbol{k}}\left[S(k) - 1\right]e^{-i\boldsymbol{k}\cdot\boldsymbol{r}} \tag{33}$$

from the static structure factor $S(k)$ obtained in the HNC approximation mentioned above. This solution is identical to that obtained in terms of the usual way of solving the classical HNC integral equation set,[31,32] and shows a better agreement with the Monte Carlo (MC) simulation results[40] than the corresponding STLS and MHNC results shown in the same figure. The interaction energy per particle is then calculated as

$$\frac{E_{int}}{N} = \frac{n}{2}\int d\boldsymbol{r} V(r)\left[g(r) - 1\right] = \frac{1}{2}\sum_{\boldsymbol{k}} v(k)\left[S(k) - 1\right]; \tag{34}$$

the HNC approximation is known[31,32] to reproduce the MC values[40,41] within the errors of 1% in the whole fluid region in contrast to the STLS approximation which shows 5.0% underestimation of the magnitude of E_{int} at $\Gamma = 10$ as compared to the MC value.[19,42,43]

The LFCs calculated at $\Gamma = 10$ are compared in Fig. 2 among the HNC, MHNC, and STLS results. In the limit of $k \to 0$, $G(k)$ is proportional to k^2 and the proportionality coefficient should be consistent with that evaluated from the thermodynamic function (compressibility sum rule, see below). The thermodymanic[42,43] asymptotic behavior of $G(k)$ is also illustrated in Fig. 2, showing the improvement of agreement

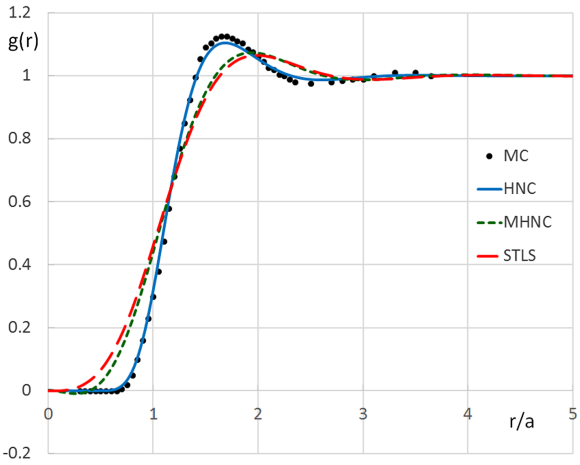

FIG. 1. Radial distribution function (RDF) at $\Gamma = 10$ in the classical limit. Blue solid line, green dotted line, and red dashed line represent the HNC, MHNC, and STLS results, respectively. Black filled circles refer to the Monte Carlo (MC) data.[40]

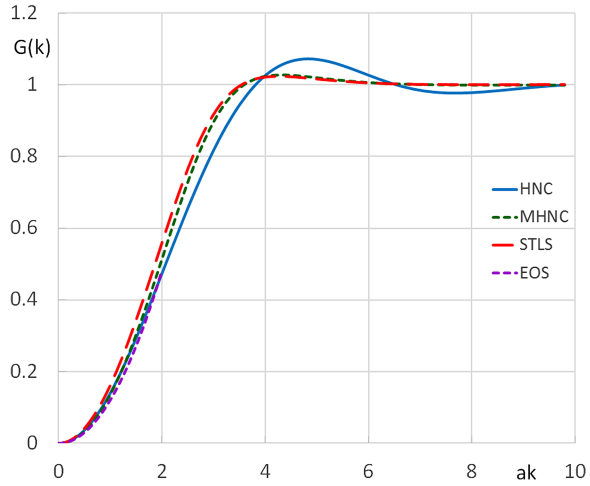

FIG. 2. Local field correction (LFC) at $\Gamma = 10$ in the classical limit. Blue solid line, green dotted line, and red dashed line represent the HNC, MHNC, and STLS results, respectively. Purple dotted line refers to the asymptotic curve obtained from the MC equation of state.[42,43]

in the cases of HNC and MHNC over the STLS result (22.2, 10.6, and 39.3 overestimations compared to the MC thermodynamic value[42,43] at $\Gamma = 10$ in the cases of HNC, MHNC, and STLS approximations, respectively). This improvement on the compressibility sum rule is due to the inclusion of the correction term $G_2(k)$ in the LFC (see also Fig. 5 below).

B. Ground state ($T = 0$)

The present HNC scheme has also been applied to the spin unpolarized ($\zeta = 0$) and fully polarized ($\zeta = 1$) electron gas system in the ground state ($T = 0$). In this case the summation over the discrete integers l in Eq. (7) is converted into the integration over the continuous variable z. Figures 3(a) and 3(b) illustrate the radial distribution functions (RDFs) calculated in the HNC and MHNC approximations for the paramagnetic state ($\zeta = 0$) at $r_s = 1$ and 10, respectively. Compared with $g(r)$ obtained through the diffusion Monte Carlo (DMC) simulation,[44] both the HNC and MHNC results show a fairly good overall agreement, but somewhat lower values and small negative region (at $r_s = 10$) near the origin ($r = 0$) since the positivity of $g(r)$ in the present HNC scheme is not guaranteed except for the classical limit. It is also noted that the extent of the negative region of $g(r)$ is reduced in comparison to that in the MCA scheme.[20]

The compressibility sum rule for the LFC is expressed by

$$\lim_{k\to 0}[-v(k)G(k)] = \frac{\partial^2}{\partial n^2}\left(\frac{F_{xc}}{V}\right), \tag{35}$$

where F_{xc}/V refers to the exchange-correlation free energy per volume. Figure 4 compares the compressibility coefficient for the LFC,

$$\gamma_{\mathrm{LFC}} = \lim_{k\to 0}\left[\left(\frac{k_F}{k}\right)^2 G(k)\right], \tag{36}$$

obtained in the HNC, MHNC, and STLS calculations with that calculated from the equation of state,

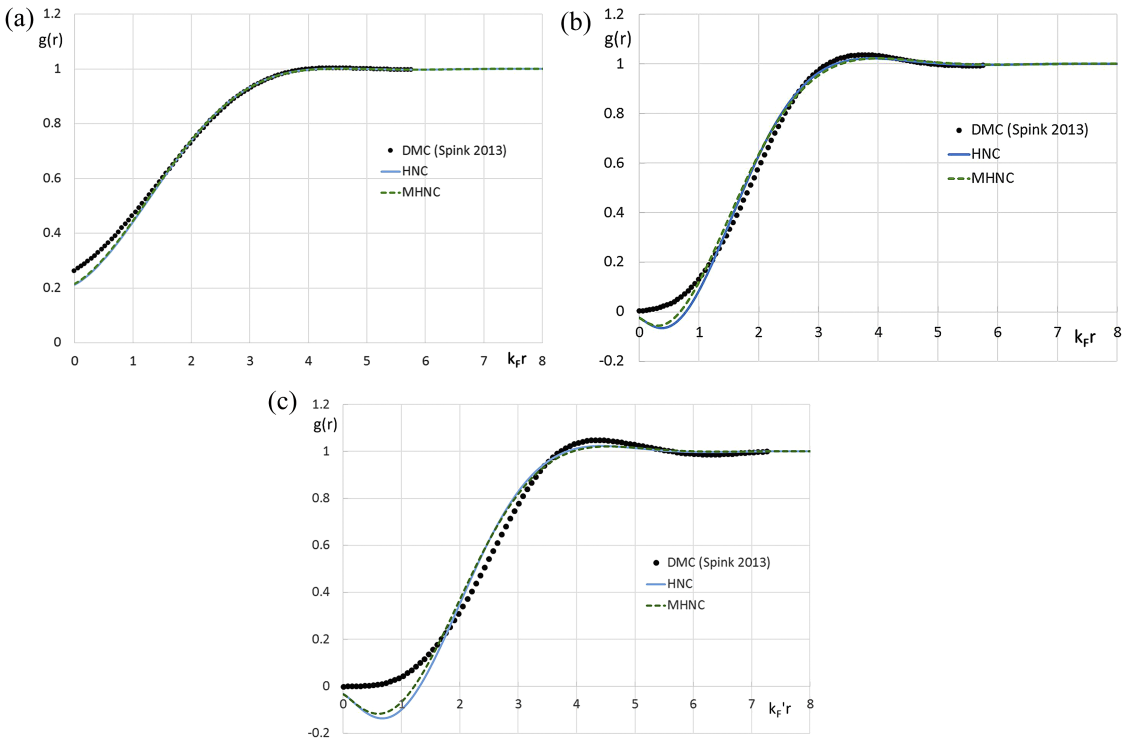

FIG. 3. RDF in the ground state ($T = 0$). Blue solid line and green dotted line represent the HNC and MHNC results, respectively. Black filled circles refer to the result obtained by the diffusion Monte Carlo (DMC) simulation.[44] (a) Calculated results at $r_s = 1$ for the paramagnetic state ($\zeta = 0$), where $k_F = (3\pi^2 n)^{1/3}$. (b) Calculated results at $r_s = 10$ for the paramagnetic state ($\zeta = 0$). (c) Calculated results at $r_s = 10$ for the ferromagnetic state ($\zeta = 1$), where $k_F' = (6\pi^2 n)^{1/3}$.

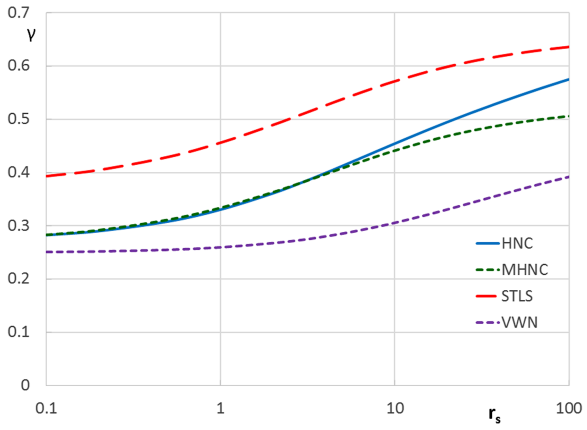

FIG. 4. Compressibility coefficient γ for $0.1 \le r_s \le 100$ at $T = 0$ and $\zeta = 0$. Blue solid line, green dotted line, and red dashed line represent the HNC, MHNC, and STLS results for $G(k)$, respectively. Purple dotted line refers to the values calculated from the exchange-correlation energies[45] fitted to the Green's function Monte Carlo (GFMC) data.[21]

$$\gamma_{\rm EOS} = -\frac{k_F^2}{4\pi e^2}\frac{\partial^2}{\partial n^2}\left(\frac{F_{xc}}{V}\right), \tag{37}$$

where the exchange-correlation energies for the ground-state paramagnetic electron gas[21] parametrized as a function of r_s by Vosko *et al.*[45] are employed. We thus observe that the self-consistency concerning the compressiblity sum rule is substantially improved in the HNC and MHNC schemes over the STLS scheme as in the classical limit. Figure 5 illustrates the division of the LFC into the $G_1(k)$ and $G_2(k)$ parts as in Eq. (26) in the HNC scheme at $r_s = 10$ and $\zeta = 0$, showing that the $G_2(k)$ works as a long-wavelength correction to the STLS-type LFC.

The interaction energy per particle in units of the Coulomb energy, $\varepsilon_{int}(r_s,\theta) = E_{int}/N(e^2/a)$, is calculated from the correlation function in terms of Eq. (34). The exchange-correlation free energy per particle in units of the Coulomb energy, $f_{xc}(r_s,\theta) = F_{xc}/N(e^2/a)$, is then evaluated through the coupling-constant integration of $\varepsilon_{int}(r_s,\theta)$ as[5,20]

$$f_{xc}(r_s,\theta) = \frac{1}{r_s}\int_0^{r_s} dx\, \varepsilon_{int}(x,\theta). \tag{38}$$

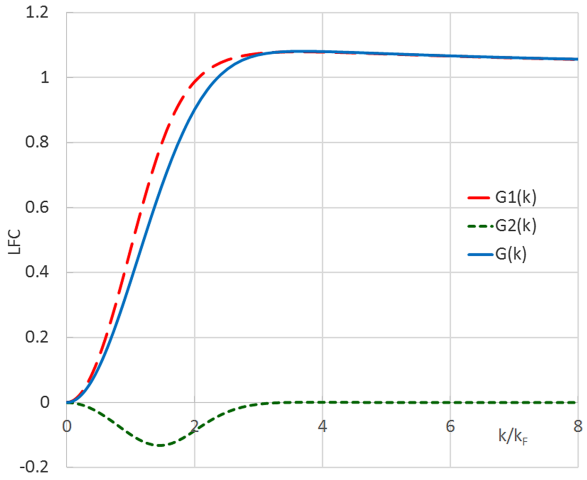

FIG. 5. Division of the LFC $G(k)$ into the $G_1(k)$ and $G_2(k)$ parts calculated in the HNC approximation at $T = 0$, $r_s = 10$, and $\zeta = 0$. Red dashed line, green dotted line, and blue solid line refer to $G_1(k)$, $G_2(k)$, and $G(k)$, respectively.

Through numerical integrations of $\varepsilon_{int}(r_s,\theta)$ calculated in the HNC and MHNC schemes for $r_s \le 100$ (data on 30 points shown in the supplementary material), we have obtained the values of the exchange-correlation energy ε_{xc} (that is, f_{xc} at $T = 0$) in the paramagnetic and ferromagnetic states, which are listed in Tables I and II, respectively. In these tables the ε_{xc} values obtained by various quantum Monte Carlo (QMC) calculations[21,44,46] are also listed in addition to the HNC, MHNC, MCA,[20] and STLS[13,14] values. As seen in Table I, the HNC values of ε_{xc} in the paramagnetic state somewhat underestimate (overestimate in the magnitude) the QMC values, but the deviations from the best (i.e., lowest) values of GFMC or DMC are less than 1% over the whole fluid region ($r_s \lesssim 100$). Considering that the VMC and fixed-node DMC calculations give upper bounds to the exact ground-state energy, this feature in the HNC approximation seems fairly well. The STLS (and MHNC) calculations show very good agreement with the QMC results at metallic densities of electrons ($2 \lesssim r_s \lesssim 6$), which is due to a fortunate cancellation of errors (see below). In the case of the ferromagnetic state, on the other hand, the deviations of the HNC values of ε_{xc} from the QMC values amount to about 2% for $4 \lesssim r_s \lesssim 8$. This underestimation of ε_{xc} in the HNC approximation can be attributed to the overestimation of the exchange-correlation hole in the short-range regime when two electrons with parallel spins approach each other. This defect in the HNC approximation may be observed in Fig. 3(c), where the RDF at $r_s = 10$ in the ferromagnetic state shows a deeper negative region around the origin than in the paramagnetic state. It is supposed that the HNC scheme describes the correlation hole due to the Coulomb repulsion very accurately, as seen in the classical limit (Fig. 1), but when the exchange (Pauli) hole predominates, its description for the total exchange-correlation hole would lead to some overcounting. This would also explain the reason why the STLS approximation, which describes the correlation hole with reduced degree, gives an accurate evaluation for the exchange-correlation energies at metallic densities. In the strong-coupling regime ($r_s \gtrsim 10$) near the Wigner crystallization, in contrast, the correlation

TABLE I. Negative of exchange-correlation energy per particle in units of e^2/a, $-\varepsilon_{xc}$, for various values of r_s in the paramagnetic state ($\zeta = 0$) at $T = 0$. The HNC, MHNC, MCA,[20] and STLS[13,14] results are compared with the variational Monte Carlo (VMC),[46] the diffusion Monte Carlo (DMC),[44,46] and the Green's function Monte Carlo (GFMC)[21] results. The symbol "· · ·" means that the corresponding values are not available.

r_s	VMC[46]	DMC[46]	DMC[44]	GFMC[21]	HNC	MHNC	MCA	STLS
0.5	· · ·	· · ·	0.495	· · ·	0.499	0.498	0.498	0.497
1.0	0.511	0.514	0.517	0.518	0.522	0.521	0.521	0.519
2.0	0.542	0.546	0.548	0.548	0.553	0.552	0.552	0.548
3.0	0.567	0.570	0.570	· · ·	0.575	0.573	0.574	0.569
4.0	0.583	0.589	· · ·	· · ·	0.592	0.589	0.592	0.585
5.0	0.596	0.599	0.600	0.599	0.606	0.603	0.606	0.598
8.0	0.626	0.630	· · ·	· · ·	0.636	0.631	0.637	0.626
10.0	0.641	0.646	0.646	0.644	0.650	0.645	0.652	0.639
20.0	· · ·	· · ·	0.691	0.688	0.693	0.685	0.697	0.678
50.0	· · ·	· · ·	· · ·	0.743	0.743	0.730	0.748	0.721
100.0	· · ·	· · ·	· · ·	0.777	0.774	0.756	0.779	0.746

TABLE II. Negative of exchange-correlation energy per particle in units of e^2/a, $-\varepsilon_{xc}$, for various values of r_s in the ferromagnetic state ($\zeta = 1$) at $T = 0$. The HNC, MHNC, MCA,[20] and STLS[13,14] results are compared with the VMC,[46] DMC,[44,46] and GFMC[21] results. The symbol "· · ·" means that the corresponding values are not available.

r_s	VMC[46]	DMC[46]	DMC[44]	GFMC[21]	HNC	MHNC	MCA	STLS
0.5	· · ·	· · ·	0.596	· · ·	0.600	0.600	0.600	0.598
1.0	0.604	0.606	0.608	· · ·	0.613	0.613	0.613	0.611
2.0	0.619	0.622	0.624	0.625	0.632	0.631	0.632	0.628
3.0	0.632	0.633	0.637	· · ·	0.646	0.644	0.646	0.641
4.0	0.640	0.643	· · ·	· · ·	0.656	0.654	0.658	0.651
5.0	0.650	0.651	0.654	0.654	0.665	0.663	0.667	0.659
8.0	0.669	0.671	· · ·	· · ·	0.685	0.681	0.688	0.676
10.0	0.679	0.681	0.683	0.682	0.695	0.690	0.698	0.685
20.0	· · ·	· · ·	0.714	0.713	0.724	0.717	0.730	0.711
50.0	· · ·	· · ·	· · ·	0.755	0.761	0.749	0.768	0.740
100.0	· · ·	· · ·	· · ·	0.785	0.785	0.768	0.791	0.758

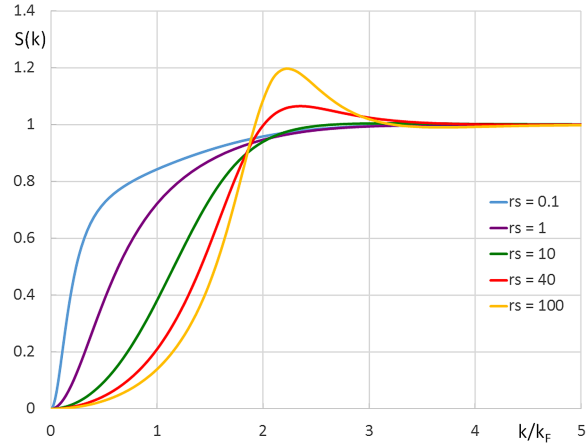

FIG. 6. Static structure factors calculated in the HNC approximation at $\theta = 1$ and $\zeta = 0$. Blue, purple, green, red, and orange curves refer to the results for $S(k)$ at $r_s = 0.1$, 1, 10, 40, and 100, respectively.

effect becomes dominant and the HNC description becomes superior to the STLS one. It is also noted that the effect by the negative region of $g(r)$ around $r \sim 0$ on the interaction energy E_{int} is much smaller than the effect due to the inaccuracy of $S(k)$ in the long-wavelength ($k \to 0$) region because of the contrast between $V(r) \propto 1/r$ and $v(k) \propto 1/k^2$ in Eq. (34) for the Coulombic system. In order to resolve this problem about the underestimation of $g(r)$ in the short-range region, we would need to incorporate the frequency-dependent LFC in the fully quantum-mechanical framework of strong-coupling theory.

C. Finite temperatures

We have performed the MHNC and HNC calculations for the spin unpolarized ($\zeta = 0$) and fully polarized ($\zeta = 1$) electron liquids at $\theta = 0.2$, 1, and 5 to obtain $S(k)$ and $G(k)$ in the density range of $r_s \leq 100$ (totally 77 points at each ζ). The numerical procedure to obtain the self-consistent solution is similar to that in the STLS case[13,14,47] in which the l summation in Eq. (7) was retained up to $|l| = 1000$. We first carried out the MHNC calculations starting with a small value of r_s at each θ and using the convergent $G(k)$ as the initial value for the calculation at larger r_s. The HNC calculations were next performed using the MHNC solution to $G(k)$ as the initial guess at the same values of θ and r_s. The RDF and the interaction energy were then calculated according to Eqs. (33) and (34). The HNC and MHNC data for ε_{int} are compiled in the supplementary material.

Figure 6 illustrates the HNC results of the static structure factor $S(k)$ for various values of r_s at $\theta = 1$ in the paramagnetic state ($\zeta = 0$). These results are compared well with the PIMC results[22] in Fig. 7, indicating a good accuracy of the HNC approximation in the intermediate to long wavelength regions. The HNC and MHNC results for RDF $g(r)$ at $\theta = 1$, $r_s = 10$, and $\zeta = 0$ are depicted and compared to the PIMC result in Fig. 8, which show a small negative region near the origin analogous to that in the ground state (see Fig. 3). The estimated values of compressibility coefficient γ_{LFC}, Eq. (36), in the HNC and MHNC approximations are depicted in Fig. 9 as functions of r_s at $\theta = 1$ and $\zeta = 0$, showing a reasonable comparison with γ_{EOS} (Eq. (37); see also Eq. (41) below) as well as in the ground-state case (Fig. 4) in the light of relatively small impact on $G(k)$ (see Fig. 2).

D. Parametrized equation of state

Using 107 HNC values of ε_{int} calculated for $r_s \leq 100$ at $\theta = 0$, 0.2, 1, and 5 each in the paramagnetic ($\zeta = 0$) and ferromagnetic ($\zeta = 1$) states (see the supplementary material), fitting expressions,

$$\varepsilon_{int}(r_s, \theta, i) = -\frac{a_i(\theta) + b_i(\theta) r_s^{1/2} + c_i(\theta) r_s}{1 + d_i(\theta) r_s^{1/2} + e_i(\theta) r_s}, \tag{39}$$

have been constructed as functions of r_s and θ, where $i = 0$ and 1 refer to $\zeta = 0$ and 1, respectively. The coefficients $a_i - e_i$ in Eq. (39) are parametrized as functions of θ in a universal form as

$$f(\theta) = F(\theta) \frac{1 + x_2\theta^2 + x_3\theta^3 + x_4\theta^4}{1 + y_2\theta^2 + y_3\theta^3 + y_4\theta^4}, \tag{40}$$

where the values of x_j and y_j ($j = 2,3,4$) and the functional forms of $F(\theta)$ are tabulated in Table III, and the form of the exchange (Hartree-Fock) contribution $a_i(\theta)$ is employed from the expression proposed by Perrot and Dharma-wardana.[8] This fitting formula, which has been constructed with the Monte Carlo optimization, reproduces the 107 HNC values of ε_{int} in the paramagnetic state with the mean absolute relative errors of 0.18% and the maximum relative errors of 1.50%; in the case of the ferromagnetic state, these errors are 0.15% and 0.94%, respectively. In the classical limit ($\theta \to \infty$), the expressions Eqs. (39) and (40) reproduce the HNC values[31,32] for $\Gamma \leq 200$ with digressions of less than 0.74%, and are reduced to the Debye-Hückel form[5,10] in the weak-coupling limit ($\Gamma \to 0$).

The expression for the exchange-correlation free energy f_{xc} is then obtained by performing the coupling-constant integration as prescribed in Eq. (38). We thus find

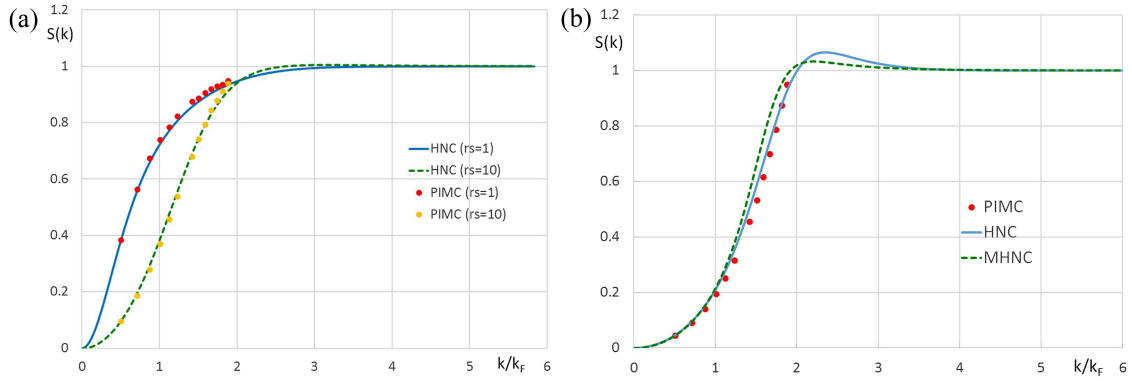

FIG. 7. Comparison of the static structure factors calculated in the HNC approximation and by the path integral Monte Carlo (PIMC) simulation[22] for various values of r_s at $\theta = 1$ and $\zeta = 0$. (a) Blue solid curve and green dotted curve refer to the HNC results at $r_s = 1$ and 10, respectively; red and orange filled circles refer to the PIMC results at $r_s = 1$ and 10, respectively. (b) Results at $r_s = 40$, where the blue solid curve, green dotted curve, and red filled circles refer to the HNC, MHNC, and PIMC results, respectively.

$$f_{xc}(r_s,\theta,i) = -\frac{c_i}{e_i} - \frac{2}{e_i}\left(b_i - \frac{c_i d_i}{e_i}\right) r_s^{-1/2} - \frac{1}{e_i r_s}\left[\left(a_i - \frac{c_i}{e_i}\right) - \frac{d_i}{e_i}\left(b_i - \frac{c_i d_i}{e_i}\right)\right] \ln\left|e_i r_s + d_i r_s^{1/2} + 1\right| + \frac{2}{e_i(4e_i - d_i^2)^{1/2} r_s}\left[d_i\left(a_i - \frac{c_i}{e_i}\right) + \left(2 - \frac{d_i^2}{e_i}\right)\left(b_i - \frac{c_i d_i}{e_i}\right)\right]\left\{\tan^{-1}\left[\frac{2e_i r_s^{1/2} + d_i}{(4e_i - d_i^2)^{1/2}}\right] - \tan^{-1}\left[\frac{d_i}{(4e_i - d_i^2)^{1/2}}\right]\right\} \quad (41)$$

for $i = 0$ (paramagnetic state) and 1 (ferromagnetic state). The normalized exchange-correlation free energies f_{xc} in the HNC approximation are illustrated in Fig. 10 as functions of r_s. In Fig. 10(a) for the paramagnetic state at $\theta = 1$, the HNC values of f_{xc} for $0.01 \le r_s \le 100$ are compared with the values obtained by other methods such as the MCA,[20] the STLS approximation,[13,14] the improved parametrization based on the STLS values (iSTLS),[48] the Vashishta-Singwi (VS) approximation,[17] the classical-map HNC (CHNC) approximation,[34,35] and the PIMC[22,24] based parametrization by Karasiev *et al.* (KSDT).[25] It is observed in Fig. 10(a) that the overall agreements among all the fitting formulas are fairly good, except for the digressions by the VS approximation and the CHNC approximation for $1 \lesssim r_s \lesssim 10$. It is noted here that the iSTLS parametrization[48] was performed to improve the defects in the original STLS-based parametrization[13,14] in the strongly degenerate ($\theta \ll 1$) regime and in the strong-coupling ($r_s, \Gamma \gg 1$) regime with the aid of known asymptotic behaviors.[5] The CHNC results may contain some inaccuracies for $S(k)$ in the intermediate to long wavelength regions.

Very recently, after the present work was complete, an improved result for f_{xc} on the basis of finite-size corrected (FSC) QMC (PB-PIMC and CPIMC) simulations has been reported.[29] Figure 10(b) compares the results of f_{xc} by the HNC and KSDT parametrizations with the FSC-QMC based fitting in the paramagnetic state as the functions of

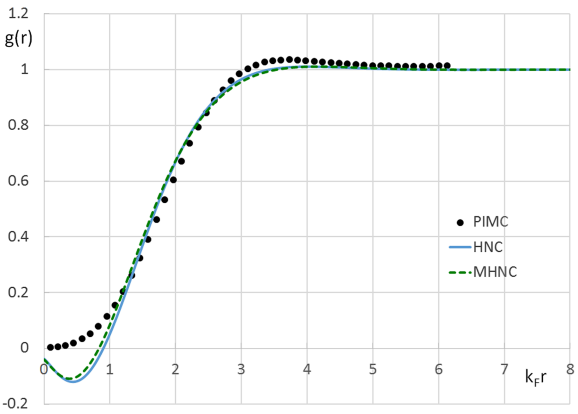

FIG. 8. RDF at $\theta = 1$ and $r_s = 10$ in the paramagnetic state ($\zeta = 0$). Blue solid line and green dotted line represent the HNC and MHNC results, respectively. Black filled circles refer to the result obtained by the PIMC simulation.[22]

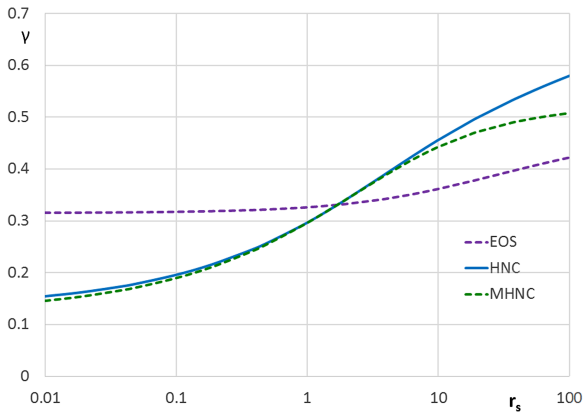

FIG. 9. Compressibility coefficient γ for $0.01 \le r_s \le 100$ at $\theta = 1$ and $\zeta = 0$. Blue solid line and green dotted line represent the HNC and MHNC results obtained via Eq. (36) from $G(k)$, respectively. Purple dotted line refers to the values calculated via Eq. (37) from the fitting formula for the exchange-correlation free energies (Eq. (41)).

TABLE III. Values of x_j and y_j (j = 2,3,4) and functional forms of $F(\theta)$ in Eq. (40) for the coefficients $a_i - e_i$ (i = 1, 2) appearing in Eq. (39). The symbol "· · ·" means that the corresponding terms have not been adopted in the approximations.

$f(\theta)$	$F(\theta)$	x_2	x_3	x_4	y_2	y_3	y_4
$a_0(\theta)$	$0.458\,165\tanh(1/\theta)$	4.058 17	−0.123 027	2.271 33	8.310 51	· · ·	5.1105
$b_0(\theta)$	$0.529\,835 d_0(\theta)$	13.397 7	2.742 82	· · ·	8.256 68	2.234 50	· · ·
$c_0(\theta)$	$0.860\,254 e_0(\theta)$	0.987 103	0.369 317	· · ·	1.048 62	0.353 894	· · ·
$d_0(\theta)$	$0.547\,950\tanh(1/\theta^{1/2})$	6.564 92	126.406	1.790 76	1.0	75.698 2	1.0
$e_0(\theta)$	$0.399\,854\tanh(1/\theta)$	1.302 60	−0.495 918	1.964 24	1.0	1.105 77	1.0
$a_1(\theta)$	$1.259\,92 a_0(0.629\,961\theta)$	· · ·	· · ·	· · ·	· · ·	· · ·	· · ·
$b_1(\theta)$	$0.607\,303 d_1(\theta)$	5.020 70	1.759 51	· · ·	3.387 78	1.644 93	· · ·
$c_1(\theta)$	$0.855\,862 e_1(\theta)$	0.757 902	0.357 122	· · ·	0.802 781	0.340 461	· · ·
$d_1(\theta)$	$0.547\,458\tanh(1/\theta^{1/2})$	−2.683 86	134.934	1.794 46	1.0	75.914 4	1.0
$e_1(\theta)$	$0.338\,480\tanh(1/\theta)$	1.871 25	−1.905 19	2.282 95	1.0	0.157 029	1.0

r_s at θ = 1, 4, and 8, where the latter QMC simulations were carried out for $\theta \geq 0.5$ and $0.1 \leq r_s \leq 10$. It is observed in this figure that the HNC results overestimate the magnitude of $|f_{xc}|$ by about 2% compared to the FSC-QMC results for $1 \lesssim r_s \lesssim 10$ at $\theta = 1$. On the other hand, the KSDT parametrization overestimates the $|f_{xc}|$ values of FSC-QMC by 7%–10% for $0.1 \lesssim r_s \lesssim 1$ at θ = 4 and 8.

As for the ferromagnetic state, the HNC results for f_{xc} at $\theta = 1$ are compared in Fig. 10(c) with the MCA,[20] the CHNC,[34,35] and the PIMC-based parametrization (KSDT)[25] results. In contrast to the paramagnetic case at $\theta = 1$, the HNC and MCA results deviate from the KSDT results more substantially. In the weak-coupling (i.e., high-density) regime ($r_s \lesssim 1$), there remains a slight deviation up to $r_s = 0.01$. In the strong-coupling regime ($1 \lesssim r_s \lesssim 100$), the difference (e.g., 5.5% at $r_s = 10$ between the HNC and KSDT results) is larger than expected from the comparisons between the HNC and simulation results in the classical and degenerate limits. Even considering the fact that the HNC approximation may underestimate the QMC values of f_{xc} by about 2% in the

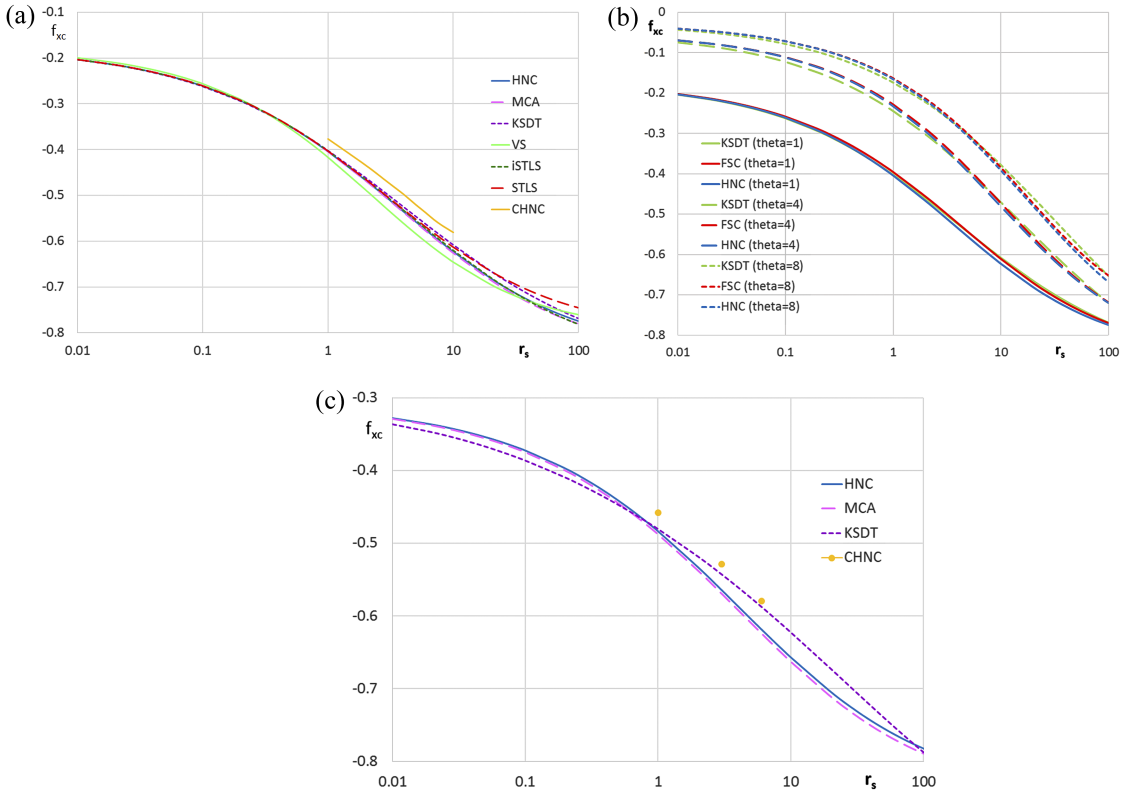

FIG. 10. Exchange-correlation free energies per particle in units of e^2/a, f_{xc}, as functions of r_s. (a) Paramagnetic state ($\zeta = 0$) at $\theta = 1$; the HNC, MCA,[20] STLS,[13,14] iSTLS,[48] Vashishta-Singwi (VS),[17] classical-map HNC (CHNC),[34,35] and PIMC-based fitting (KSDT)[25] results are represented by the blue solid line, pink dashed line, red dashed line, green dotted line, yellow-green solid line, orange solid line, and purple dotted line, respectively. (b) Comparison of the HNC and KSDT results with the finite-size corrected (FSC) QMC results[29] for the paramagnetic state at θ = 1, 4, and 8; blue, green, and red curves refer to the HNC, KSDT, and FSC-QMC results, respectively; solid, dashed, and dotted lines represent the results for θ = 1, 4, and 8, respectively. (c) Ferromagnetic state ($\zeta = 1$) at $\theta = 1$, where it is noted that "$\theta = 1$" in the present study corresponds to $t = 2^{-2/3} = 0.629\,961$ in the KSDT fitting[25] for the ferromagnetic state; the HNC, MCA, CHNC, and KSDT results are represented by blue solid line, pink dashed line, orange filled circles, and purple dotted line, respectively.

ferromagnetic state for $\theta \to 0$ and also some errors in the fitting procedures, we may thus propose that the re-examination on the exchange-correlation free energies for the spin-polarized electron gas system at finite temperatures should be performed from both sides of QMC simulations and analytic approaches.

We have thus derived the analytic expressions for ε_{int} and f_{xc} as the functions of θ and r_s both in the paramagnetic ($\zeta = 0$) and ferromagnetic ($\zeta = 1$) states. In order to obtain the expressions available at any spin polarization ($0 < \zeta < 1$), we can use the interpolation scheme developed in the MCA study.[20] It is expected that the MCA interpolation function which depends on ζ, r_s, and θ would work well also in the HNC case, because the differences in ε_{int} and f_{xc} between the HNC and MCA approximations are very minor over the whole $r_s - \theta$ regions and the functional dependence on the degree of spin polarization is expected to be smooth and simple.

IV. CONCLUDING REMARKS

The present work has performed the calculations for the correlational and thermodynamic functions of finite-temperature electron liquids in the paramagnetic and ferromagnetic states over a wide range of density and temperature parameters on the basis of the HNC and MHNC approximations. Primary attention has been focused upon the construction of accurate equations of state for homogeneous electron fluid which can be used as the input for finite-temperature DFT calculations with good accuracy comparable to those obtained through QMC simulations. The accuracies for the exchange-correlation free energies achieved in the present HNC study are superior to those in the CHNC[34,35] and VS[17] schemes, as seen in Fig. 10(a). As compared to the earlier STLS results,[13,14] the improvements of the consistency in the compressibility sum rule and of the correlation energy in the strong-coupling regime have been observed. Further, the improvements of the RDF in the short-range region and of the correlation energy in the intermediate-coupling regime have been found over the MCA results.[20] The accurate knowledge of $G(k)$ is essential for constructing the dielectric screening function of electrons $\epsilon(k, \omega)$[5,10] and the associated static structure factor $S(k)$; the information about $S(k)$ has recently been utilized to perform the finite-size correction for QMC thermodynamic data.[29] The information on $g(r)$ or $S(k)$ of the uniform electron gas can also provide the key input to the finite-temperature DFT calculations for inhomogeneous systems in which the density-gradient corrections may be taken into account.[49]

The parametrized expression for the exchange-correlation free energy obtained in the present HNC study is expected to reproduce the exact values of f_{xc} with the relative errors of less than a few % over the whole $n - T$ region of the fluid phase in the paramagnetic and ferromagnetic states. The probable digressions in the intermediate-coupling regime would be ascribed to the small negative region of $g(r)$ near the origin, but the influence of this error upon thermodynamic functions is minor in comparison to that associated with $S(k)$ in the long-wavelength region. Through comparison with earlier studies, a number of proposed expressions for f_{xc} thus appear to converge well to a common (probably correct) evaluation in the paramagnetic state. On the other hand, even considering the expected 2% – 3% underestimation for f_{xc} (overestimation for $|f_{xc}|$) by the present HNC scheme, the differences between the HNC and PIMC results in the intermediate-coupling ($1 \lesssim r_s \lesssim 10$) and weak-coupling ($r_s \lesssim 1$) regimes observed at $\theta = 1$ in the ferromagnetic state (Fig. 10(c)) seem to be too large, thus suggesting the necessity of further QMC studies and associated re-examination on the equation of state.

SUPPLEMENTARY MATERIAL

See supplementary material for the interaction energies of electron liquids at $\theta = 0$, 0.2, 1, and 5, $\zeta = 0$ and 1, and $r_s \leq 100$ calculated in the HNC and MHNC approximations.

ACKNOWLEDGMENTS

The author would like to acknowledge the Grants-in-Aid for Scientific Research (Grant No. 26460035) from the Ministry of Education, Culture, Sports, Science and Technology (MEXT). The numerical computations in the present work were carried out by the IBM eServer p7 model 755 at the Information Science and Technology Center of Kobe University.

[1] S. P. Regan, K. Falk, G. Gregori, P. B. Radha, S. X. Hu, T. R. Boehly, B. J. B. Crowley, S. H. Glenzer, O. L. Landen, D. O. Gericke, T. Döppner, D. D. Meyerhofer, C. D. Murphy, T. C. Sangster, and J. Vorberger, Phys. Rev. Lett. **109**, 265003 (2012).
[2] L. B. Fletcher, A. L. Kritcher, A. Pak, T. Ma, T. Döppner, C. Fortmann, L. Divol, O. S. Jones, O. L. Landen, H. A. Scott, J. Vorberger, D. A. Chapman, D. O. Gericke, B. A. Mattern, G. T. Seidler, G. Gregori, R. W. Falcone, and S. H. Glenzer, Phys. Rev. Lett. **112**, 145004 (2014).
[3] M. W. C. Dharma-wardana, Computation **4**, 16 (2016).
[4] V. V. Karasiev, L. Calderin, and S. B. Trickey, Phys. Rev. B **93**, 063207 (2016).
[5] S. Ichimaru, H. Iyetomi, and S. Tanaka, Phys. Rep. **149**, 91 (1987).
[6] U. Gupta and A. K. Rajagopal, Phys. Rev. A **22**, 2792 (1980).
[7] U. Gupta and A. K. Rajagopal, Phys. Rep. **87**, 259 (1982).
[8] F. Perrot and M. W. C. Dharma-wardana, Phys. Rev. A **30**, 2619 (1984).
[9] D. G. Kanhere, P. V. Panat, A. K. Rajagopal, and J. Callaway, Phys. Rev. A **33**, 490 (1986).
[10] S. Ichimaru, Rev. Mod. Phys. **54**, 1017 (1982).
[11] R. G. Dandrea, N. W. Ashcroft, and A. E. Carlsson, Phys. Rev. B **34**, 2097 (1986).
[12] K. S. Singwi, M. P. Tosi, R. H. Land, and A. Sjölander, Phys. Rev. **176**, 589 (1968).
[13] S. Tanaka and S. Ichimaru, J. Phys. Soc. Jpn. **55**, 2278 (1986).
[14] S. Tanaka, S. Mitake, and S. Ichimaru, Phys. Rev. B **32**, 1896 (1985).
[15] H. K. Schweng and H. M. Böhm, Phys. Rev. B **48**, 2037 (1993).
[16] P. Vashishta and K. S. Singwi, Phys. Rev. B **6**, 875 (1972).
[17] T. Sjostrom and J. Dufty, Phys. Rev. B **88**, 115123 (2013).
[18] K. Tago, K. Utsumi, and S. Ichimaru, Prog. Theor. Phys. **65**, 54 (1981).
[19] X.-Z. Yan and S. Ichimaru, J. Phys. Soc. Jpn. **56**, 3853 (1987).
[20] S. Tanaka and S. Ichimaru, Phys. Rev. B **39**, 1036 (1989).
[21] D. M. Ceperley and B. J. Alder, Phys. Rev. Lett. **45**, 566 (1980).
[22] E. W. Brown, B. K. Clark, J. L. DuBois, and D. M. Ceperley, Phys. Rev. Lett. **110**, 146405 (2013).
[23] D. M. Ceperley, J. Stat. Phys. **63**, 1237 (1991).
[24] E. W. Brown, J. L. DuBois, M. Holzmann, and D. M. Ceperley, Phys. Rev. B **88**, 081102(R) (2013).
[25] V. V. Karasiev, T. Sjostrom, J. Dufty, and S. B. Trickey, Phys. Rev. Lett. **112**, 076403 (2014).
[26] T. Dornheim, T. Schoof, S. Groth, A. Filinov, and M. Bonitz, J. Chem. Phys. **143**, 204101 (2015).

[27] S. Groth, T. Schoof, T. Dornheim, and M. Bonitz, Phys. Rev. B **93**, 085102 (2016).
[28] T. Schoof, S. Groth, J. Vorberger, and M. Bonitz, Phys. Rev. Lett. **115**, 130402 (2015).
[29] T. Dornheim, S. Groth, T. Sjostrom, F. D. Malone, W. M. C. Foulkes, and M. Bonitz, Phys. Rev. Lett. **117**, 156403 (2016).
[30] J.-P. Hansen and I. R. McDonald, *Theory of Simple Liquids*, 3rd ed. (Academic Press, London, 2006).
[31] J. F. Springer, M. A. Pokrant, and F. A. Stevens, Jr., J. Chem. Phys. **58**, 4863 (1973).
[32] K.-C. Ng, J. Chem. Phys. **61**, 2680 (1974).
[33] Ph. Choquard, in *Strongly Coupled Plasmas*, edited by G. Kalman (Plenum, New York, 1978), p. 347.
[34] M. W. C. Dharma-wardana and F. Perrot, Phys. Rev. Lett. **84**, 959 (2000).
[35] F. Perrot and M. W. C. Dharma-wardana, Phys. Rev. B **62**, 16536 (2000).
[36] S. Dutta and J. Dufty, Europhys. Lett. **102**, 67005 (2013).
[37] Y. Liu and J. Wu, J. Chem. Phys. **141**, 064115 (2014).
[38] J. L. Lantto, Phys. Rev. B **22**, 1380 (1980).
[39] J. G. Zabolitzky, Phys. Rev. B **22**, 2353 (1980).
[40] S. G. Brush, H. L. Sahlin, and E. Teller, J. Chem. Phys. **45**, 2102 (1966).
[41] J.-P. Hansen, Phys. Rev. A **8**, 3096 (1973).
[42] W. L. Slattery, G. D. Doolen, and H. E. DeWitt, Phys. Rev. A **21**, 2087 (1980).
[43] W. L. Slattery, G. D. Doolen, and H. E. DeWitt, Phys. Rev. A **26**, 2255 (1982).
[44] G. G. Spink, R. J. Needs, and N. D. Drummond, Phys. Rev. B **88**, 085121 (2013).
[45] S. H. Vosko, L. Wilk, and M. Nusair, Can. J. Phys. **58**, 1200 (1980).
[46] G. Ortiz and P. Ballone, Phys. Rev. B **50**, 1391 (1994).
[47] The convergence criterion adopted in the self-consistent integral equations for $S(k)$ and $G(k)$ at $\theta = 0$, 0.2, 1, and 5 is $\int_0^{x_{max}} dx[G_{out}(x) - G_{in}(x)]^2 < \delta$ for the input and output LFC values in the iteration process, where $x = k/k_F$ (or k/k'_F), $x_{max} = 1000.0$, $\delta = 10^{-8}$ for $r_s < 1.0$, and $\delta = 10^{-8} r_s$ for $r_s \geq 1.0$.
[48] S. Ichimaru, Rev. Mod. Phys. **65**, 255 (1993); S. Tanaka, "Improved equation of state for finite-temperature spin-polarized electron liquids on the basis of Singwi-Tosi-Land-Sjolander approximation" (unpublished).
[49] J. P. Perdew and Y. Wang, Phys. Rev. B **46**, 12947 (1992).